

Improved satellite retrievals of NO<sub>2</sub> and SO<sub>2</sub> over the Canadian oil sands

C. A. McLinden et al.

This discussion paper is/has been under review for the journal Atmospheric Chemistry and Physics (ACP). Please refer to the corresponding final paper in ACP if available.

# Improved satellite retrievals of NO<sub>2</sub> and SO<sub>2</sub> over the Canadian oil sands and comparisons with surface measurements

C. A. McLinden<sup>1</sup>, V. Fioletov<sup>1</sup>, K. F. Boersma<sup>2,3</sup>, S. K. Kharol<sup>4</sup>, N. Krotkov<sup>5</sup>,  
L. Lamsal<sup>5</sup>, P. A. Makar<sup>1</sup>, R. V. Martin<sup>4,6</sup>, J. P. Veefkind<sup>2,7</sup>, and K. Yang<sup>5,8</sup>

<sup>1</sup>Environment Canada, Toronto, Canada

<sup>2</sup>Royal Netherlands Meteorological Institute (KNMI), De Bilt, the Netherlands

<sup>3</sup>Eindhoven University of Technology, Fluid Dynamics Lab, Eindhoven, the Netherlands

<sup>4</sup>Dalhousie University, Department of Physics and Atmospheric Science, Halifax, Nova Scotia, Canada

<sup>5</sup>Laboratory for atmospheric chemistry and dynamics, NASA Goddard Space Flight Center, Greenbelt, MD, USA

<sup>6</sup>Harvard-Smithsonian Center for Astrophysics, Cambridge, MA, USA

<sup>7</sup>Civil Engineering and Geosciences, Delft University of Technology, Delft, the Netherlands

<sup>8</sup>Department of Atmospheric and Oceanic Sciences, University of Maryland, College Park, Maryland, USA

Title Page

Abstract

Introduction

Conclusions

References

Tables

Figures

⏪

⏩

◀

▶

Back

Close

Full Screen / Esc

Printer-friendly Version

Interactive Discussion

Received: 19 July 2013 – Accepted: 30 July 2013 – Published: 21 August 2013

Correspondence to: C. A. McLinden (chris.mclinden@ec.gc.ca)

Published by Copernicus Publications on behalf of the European Geosciences Union.

ACPD

13, 21609–21664, 2013

**Improved satellite retrievals of NO<sub>2</sub> and SO<sub>2</sub> over the Canadian oil sands**

C. A. McLinden et al.

Title Page

Abstract

Introduction

Conclusions

References

Tables

Figures



Back

Close

Full Screen / Esc

Printer-friendly Version

Interactive Discussion



## Abstract

Satellite remote sensing is increasingly being used to monitor air quality over localized sources such as the Canadian oil sands. Following an initial study, significant low biases have been identified in current NO<sub>2</sub> and SO<sub>2</sub> retrieval products from the Ozone Monitoring instrument (OMI) satellite sensor over this location resulting from a combination of its rapid development and small spatial scale. Air mass factors (AMFs) used to convert line-of-sight “slant” columns to vertical columns were re-calculated for this region based on updated and higher resolution input information including absorber profiles from a regional scale (15 km × 15 km resolution) air quality (AQ) model, higher spatial and temporal resolution surface reflectivity, and an improved treatment of snow. The overall impact of these new Environment Canada (EC) AMFs led to substantial increases in the peak NO<sub>2</sub> and SO<sub>2</sub> average vertical column density (VCD), occurring over an area of intensive surface mining, by factors of 2 and 1.4, respectively, relative to estimates made with previous AMFs. Comparisons are made with long-term averages of NO<sub>2</sub> and SO<sub>2</sub> from in-situ surface monitors by using the AQ model to map the OMI VCDs to surface concentrations. This new OMI-EC product is able to capture the spatial distribution of the in-situ instruments (slopes of 0.7 to 1.0; correlation coefficients of 0.9). The concentration absolute values from surface network observations were in reasonable agreement, with OMI-EC NO<sub>2</sub> and SO<sub>2</sub> biased low by roughly 30%. Several complications were addressed including correction for the interference effect in the surface NO<sub>2</sub> instruments and smoothing and clear-sky biases in the OMI measurements. Overall these results highlight the importance of using input information that accounts for the spatial and temporal variability of the location of interest when performing retrievals.

## Improved satellite retrievals of NO<sub>2</sub> and SO<sub>2</sub> over the Canadian oil sands

C. A. McLinden et al.

Title Page

Abstract

Introduction

Conclusions

References

Tables

Figures



Back

Close

Full Screen / Esc

Printer-friendly Version

Interactive Discussion



## 1 Introduction

Space-based measurements of the near-surface atmospheric composition, or air quality (AQ), from near-UV-to-near-IR spectra have blossomed over the past two decades from relatively crude, research-grade products to refined, operational products suitable for monitoring and assimilation (e.g., Miyazaki et al., 2012). These products include tropospheric vertical column densities of NO<sub>2</sub>, SO<sub>2</sub>, CO, HCHO, and aerosol optical depth from nadir-viewing instruments that measure backscattered sunlight (e.g., Martin, 2008). Furthermore, through the fusion of satellite data and models, fundamental quantities crucial to air quality such as surface concentration (Lamsal et al., 2008) and emission rates (Streets et al., 2013) are now being derived from these less familiar vertically-integrated quantities.

This category of sensor began with the GOME (Global Ozone Monitoring Experiment) instrument (Burrows et al., 1999) and continued with SCIAMACHY (SCanning Imaging Absorption spectroMeter for Atmospheric CartographY, 2002–2012) (Bovensmann, 1999), OMI (Ozone Monitoring Instrument, 2004–present) (Levelt et al., 2006), and the operational GOME-2 (2006–present, 2012–present) instruments. Collectively these instruments have provided invaluable information on distributions and trends in NO<sub>2</sub> and SO<sub>2</sub> despite the complexities associated with the inversion of these spectra. Applications of these data to air quality issues are numerous and span wide spatial and temporal scales.

More recently these data have been applied to the analysis of localized sources whose spatial extent is comparable to that of a individual resolution element, or pixel (Beirle et al., 2011; Fioletov et al., 2011). One high-profile example is the Canadian oil sands (McLinden et al., 2012). This area in the northeast corner of the province of Alberta contains a vast deposit of hydrocarbons, including an equivalent of 170 billion barrels (roughly  $2.7 \times 10^7 \text{ m}^3$ ) of oil in the form of bitumen, a viscous form of petroleum. Production has increased rapidly from about 0.6 million barrels per day (mBPD) in 1998 to 2 mBPD in 2012 and with a further doubling expected over the next decade (ERCB,

## Improved satellite retrievals of NO<sub>2</sub> and SO<sub>2</sub> over the Canadian oil sands

C. A. McLinden et al.

Title Page

Abstract

Introduction

Conclusions

References

Tables

Figures



Back

Close

Full Screen / Esc

Printer-friendly Version

Interactive Discussion







## 2.3 Atmospheric chemistry models

This study also makes extensive use two atmospheric chemistry models. The first is the Global Environmental Multi-scale–Modelling Air quality and Chemistry (GEM-MACH). GEM-MACH is the Canadian regional air quality forecast model used operationally to predict the concentrations of O<sub>3</sub>, NO<sub>2</sub>, PM<sub>2.5</sub> over North America, and the Canadian Air Quality Health Index at cities within Canada (Moran et al., 2009; Anselmo et al., 2010). The model makes use of detailed tropospheric processes for gas and particle chemistry and microphysics originating in the off-line A Unified Regional Air-quality Modelling System (AURAMS, Gong et al., 2006), but incorporated on-line into the Canadian weather forecast model (Global Environmental Multiscale model, Côté et al., 1998). A detailed description of the chemical processes found in AURAMS and GEM-MACH may also be found in Kelly et al. (2012). Both AURAMS and GEM-MACH share a sectional, speciated particle distribution – for the operational GEM-MACH forecasts used here, two bins are used, to represent particle fine and coarse modes, respectively. These results used here are from archived forecasts from 2010 to 2011 for a domain covering North America at 15 km × 15 km resolution. The emissions inventories for the model are from US EPA and Environment Canada data for the year 2006. Note that GEM-MACH at present does not include NO<sub>x</sub> sources for biomass burning and lightning.

The second is the GEOS-Chem chemical transport model (Bey et al., 2001) version v8-03-01 ([www.geos-chem.org](http://www.geos-chem.org)) driven by assimilated meteorological observations from the Goddard Earth Observing System (GEOS-5). These simulations were run at 1/2° (latitude) by 2/3° (longitude) resolution in a nested mode over a North-American grid (Chen et al., 2009; van Donkelaar et al., 2012). The model includes a detailed simulation of tropospheric ozone-NO<sub>x</sub>-hydrocarbon chemistry as well as aerosols and their precursors (Park et al., 2004). Canadian anthropogenic emissions are from the CAC inventory (<http://www.ec.gc.ca/inrp-npri>) for 2005. Emissions from open fires for individual years are from the GFED2 inventory with monthly resolution

### Improved satellite retrievals of NO<sub>2</sub> and SO<sub>2</sub> over the Canadian oil sands

C. A. McLinden et al.

Title Page

Abstract

Introduction

Conclusions

References

Tables

Figures



Back

Close

Full Screen / Esc

Printer-friendly Version

Interactive Discussion



(van der Werf et al., 2009). Lightning  $\text{NO}_x$  emissions are computed as a function of cloud top height, and are scaled globally as described by Sauvage et al. (2007) to match OTD/LIS climatological observations of lightning flashes. The global source is imposed to be  $6 \text{ Tg(N) yr}^{-1}$  (Martin et al., 2007). Higher  $\text{NO}_x$  yields per flashes are used at mid-latitudes than in the tropics (Hudman et al., 2007).

Daily output from both models are sampled at the local time of the OMI overpass, roughly 13:30 LT, and from this monthly-means are calculated.

## 2.4 OMI measurements over the oil sands

The rapid development of the oil sands raises concern over the validity of some assumptions underlying current  $\text{NO}_2$  and  $\text{SO}_2$  data products. Space-based nadir UV-sensors are generally less sensitive to an absorber located near the surface as opposed to one aloft, and thus a key parameter in the retrieval algorithm is the assumed vertical profile of the absorber. Both  $\text{NO}_2$  algorithms, the SP and DOMINO, rely on model-calculated  $\text{NO}_2$  profiles: the SP uses monthly-mean profiles from the Global Modeling Initiative (GMI) (Bucsela et al., 2013) and DOMINO uses daily output from the TM4 (Tracer Model 4) chemical transport model (Boersma et al., 2007). Both models, however, make use of emission inventories appropriate for the late 1990s when oil sands  $\text{NO}_x$  emissions were significantly smaller than current values (Boersma et al., 2007; B. Swartz, personal communication, 2012). The impact of this can be seen in the  $\text{NO}_2$  profiles from these different sources of data in the vicinity of the oil sands. Figure 2a shows the annual-mean  $\text{NO}_2$  profiles over the oil sands, sampled at the local time of the OMI overpass, from the GMI (horizontal resolution of  $2^\circ \text{ lat} \times 2.5^\circ \text{ lon}$ ) and TM4 ( $2^\circ \times 3^\circ$ ) models. Also shown for comparison are profiles from the higher resolution models discussed in Sect. 2.3, GEOS-CHEM and GEM-MACH, smoothed to match the resolution of GMI. The profiles are presented as shape-factors, which are volume mixing ratio (vmr) profiles normalized by their column-averaged vmr. The GMI and TM4 profiles show values that are significantly smaller in the PBL, by a factor of 2–3, than GEOS-CHEM and GEM-MACH and generally resemble shape factors for

near-background profiles. In fact, their absolute value in the boundary layer is only about 0.1–0.3 ppb, and so are representative of background levels. As is discussed below, the end result of this underestimate of NO<sub>2</sub> in the PBL is an underestimate of tropospheric VCDs.

Beyond the outdated emissions is the related issue of model resolution. With grid boxes in excess of 200 km (latitude) by 150 km (longitude), the GMI and TM4 models cannot resolve the surface mining region whose entirety spans 50 km by 30 km. This means the same model NO<sub>2</sub> profile may be used at both the center of emissions and 100 km away where the NO<sub>2</sub> would be at or near background levels. This issue of profile “representativeness” has been identified as a potential error source for near-point sources (Heckel et al., 2011). Figure 2b illustrates the steep horizontal gradients in the annual-mean NO<sub>2</sub> profiles from the GEM-MACH model by comparing vmr profiles at the maximum emissions with those at 10 and 50 km away.

Related concerns exist for SO<sub>2</sub> VCDs: the use of an invariant AMF, calculated for summertime conditions in the eastern US, will likely also lead to spatial and seasonal biases although in this case the sign of the bias is less apparent. On this basis it was concluded that there is a potential for significant systematic errors in these current (DOMINO and SP NO<sub>2</sub> and NASA SO<sub>2</sub>) products over the oil sands region. Thus, any quantitative assessment of these gases requires AMFs to be re-evaluated in this region accounting for both the rapidly changing emissions and their small spatial scale. Furthermore, calculating NO<sub>2</sub> and SO<sub>2</sub> AMFs in a consistent manner should increase their compatibility, possibly allowing for their ratio or differences in their spatial distributions to be used to infer additional information about the nature of sources.

Improved satellite retrievals of NO<sub>2</sub> and SO<sub>2</sub> over the Canadian oil sands

C. A. McLinden et al.

Title Page

Abstract

Introduction

Conclusions

References

Tables

Figures



Back

Close

Full Screen / Esc

Printer-friendly Version

Interactive Discussion



### 3 Air mass factors

#### 3.1 General concept

The general AMF framework used herein follows that of Palmer et al. (2001), Martin et al. (2002), and others. The AMF ( $M$ ), defined as the ratio of the SCD ( $S$ ) to the VCD ( $V$ ), or  $M = S/V$ , describes the enhancement in absorption when light traverses a slant path through a layer and represents a cornerstone of retrievals in the UV-visible portion of the spectrum. From this definition, the steps in the retrieval algorithm described in Sect. 2.2 can be expressed as,

$$V_t = \frac{S_t}{M} = \frac{S - S_s}{M} \quad (1)$$

where  $S = S_t + S_s$ , and subscripts “s” and “t” refer to stratosphere and troposphere, respectively, and  $M$  is the tropospheric AMF. Here  $S$ , determined from the spectral analysis, is the only quantity measured directly by OMI;  $S_s$  and  $M$  must be determined from a combination of statistical considerations, modelling, or assimilation. For  $\text{SO}_2$  it is assumed there is no appreciable stratospheric component ( $S_s = 0$ ).

When direct sunlight is measured, as may be the case for a ground-based spectrometer, it is straightforward to determine the path of the sunlight through the atmosphere, and hence the AMF may be deduced from purely geometrical considerations. However, when scattered sunlight is the source of information, the path is much more complex involving, in general, multiple scattering and surface reflection events. Moreover, the measured radiance will be a combination of many different paths. Resolving this requires radiative transfer models capable of simulating the multiple-scattering and absorption processes.

The distribution of scattered light, including nadir radiances (and thus AMFs), is controlled by many factors including solar and instrument viewing geometry, surface reflectivity, aerosols and clouds, and the vertical distribution of the absorber (e.g., Martin et al., 2003). It is most convenient to account for the dependence on vertical distribution

by using a vertically-resolved AMF,  $m(z)$ , such that  $M$  represents the absorber number density weighted-average of  $m(z)$ ,

$$M = \frac{S}{V} = \frac{\int_z n(z) \cdot m(z) \cdot \alpha[T(z)] \cdot dz}{\int_z n(z) \cdot dz} \quad (2)$$

where  $n(z)$  is the absorber number density vertical profile and  $\alpha[T(z)]$  is a correction factor that accounts for the change in the absorption cross-section with temperature. For both species a correction of  $\alpha = 1 - 0.003[T(z) - T_0]$  was used where  $T_0 = 220$  K for  $\text{NO}_2$  (Boersma et al., 2004) and  $T_0 = 273$  K for  $\text{SO}_2$  correspond to the temperatures of the cross-sections used in the spectral analysis. Values of  $m(z)$  are also referred to a box-AMFs and are analogous to the scattering weights used in other studies (e.g., Martin et al., 2002) but without a normalization by a geometric AMF.

Another of the key factors in determining AMFs are clouds. Clouds behave as bright surfaces reflecting more light than that of the underlying surface. They also act to shield the sensor from any absorbers located below the cloud. The treatment of clouds used here follows the general approach used in other studies (Boersma et al., 2004; Martin et al., 2006) in which they are modelled as Lambertian reflectors located at the cloud altitude, and with an albedo of 0.8. In the case of a partially cloudy pixel, the AMF is taken as a linear combination of the cloudy and clear-sky AMF as follows,

$$M = w \cdot M_c + (1 - w) \cdot M_a \quad (3)$$

where  $w$  is the radiative cloud fraction and the subscripts “c” and “a” represent cloudy and clear-sky, respectively. The radiative cloud fraction represents the fraction of the nadir radiance that is due to the cloudy portion of the pixel. It differs from the effective (geometric) cloud fraction,  $f$ , as clouds tend to be more reflective and thus contribute disproportionately to the overall radiance. They are related by  $w = f \cdot I_c / [f \cdot I_c + (1 - f) \cdot I_a]$ , where  $I$  is the nadir radiance.

Improved satellite retrievals of  $\text{NO}_2$  and  $\text{SO}_2$  over the Canadian oil sands

C. A. McLinden et al.

Title Page

Abstract

Introduction

Conclusions

References

Tables

Figures

⏪

⏩

◀

▶

Back

Close

Full Screen / Esc

Printer-friendly Version

Interactive Discussion







## Improved satellite retrievals of NO<sub>2</sub> and SO<sub>2</sub> over the Canadian oil sands

C. A. McLinden et al.

Title Page

Abstract

Introduction

Conclusions

References

Tables

Figures

◀

▶

◀

▶

Back

Close

Full Screen / Esc

Printer-friendly Version

Interactive Discussion

the SO<sub>2</sub> spectral region (~ 315 nm). The errors introduced in OMI NO<sub>2</sub> AMFs using this MODIS product over the more rigorous bidirectional reflection distribution function (BRDF) has been examined by Zhou et al. (2010). In the summer errors are < 5 % while for lower sun angles errors of 10–20 % are possible depending on the shape of the absorbing profile.

The spatial patterns in the OMI albedos (Kleipool et al., 2008) at 342 nm and 477 nm reveals were found to be general consistent, thereby suggesting it is reasonable to simply scale the MODIS albedo by an OMI-derived ratio to arrive at a better representation of reflectivity at near-SO<sub>2</sub> wavelengths. As MODIS provides both BSA and WSA, where BSA is more appropriate for direct sunlight incident on the surface and WSA for diffuse light, a weighted average is used with the weighting determined by the model calculated fraction of downwelling irradiance that is diffuse. In this work, albedo was calculated using,

$$\alpha(\lambda; t; x, y) = [(1 - f_{\text{dif}}) \cdot \alpha_{\text{bs}}(\lambda_M; t, x, y) + f_{\text{dif}} \cdot \alpha_{\text{ws}}(\lambda_M; t, x, y)] \cdot \left[ \frac{\alpha(\lambda)}{\alpha(\lambda_M)} \right]_{\text{OMI}} \quad (4)$$

where  $\alpha_{\text{bs}}$  and  $\alpha_{\text{ws}}$  are the MODIS monthly-mean BSA and WSA at a wavelength of  $\lambda_M = 477$  nm and  $f_{\text{dif}}$  is the model-calculated (see Sect. 3.3) fraction of the total downwelling irradiance at the surface that is diffuse. The averages are calculated using 100 % snow-free scenes and were smoothed to approximate the resolution of a representative OMI pixel (15 km × 30 km). The final factor in Eq. (3) adjusts the MODIS albedo to that a wavelength more representative of the spectral region used in the analyses,  $\lambda = 440$  nm for NO<sub>2</sub> or  $\lambda = 342$  nm for SO<sub>2</sub>, using the updated Kleipool et al. (2008) OMI monthly climatology.

Examples of the MODIS-derived surface albedo (via Eq. 4) for NO<sub>2</sub> and SO<sub>2</sub> are shown in Fig. 3, along with that from the OMI-climatology, averaged over the summer (JJA). The MODIS maps for NO<sub>2</sub> albedo are for 2005 and 2011 and for SO<sub>2</sub> for 2005. The general magnitudes of the OMI reflectivity and the MODIS are similar, but the higher resolution of the MODIS clearly show the footprint of the surface mines. They

also reveal that there is an evolution with time. Also of note are the slightly larger values of albedo for SO<sub>2</sub> relative to NO<sub>2</sub> resulting from the wavelength adjustment.

### 3.2.3 Identification and treatment of snow

Owing to the large fraction of OMI observations that are made over snow in the oil sands region, roughly 40 %, it is important to address this aspect as well. Problems with UV/visible measurements over snow have been discussed in previous work (O'Byrne et al., 2010). In principle snow represents an ideal surface in that its higher reflectivity means the instrument is more sensitive to the near-surface and thus less sensitive to the shape of the absorber profile. In practice, however, complications arise due to issues with correctly identifying the presence of snow (either false positives or false negatives) and the subsequent choice of an appropriate surface albedo (snow or snow-free) for the determination of the cloud fraction and AMFs. The end result is often large errors in the cloud fraction and the use of an inappropriate surface reflectivity. The intent here is not to remedy the entirety of the problem as this requires an improved cloud fraction data product which is beyond the scope of this study. Nonetheless, two elements can be readily addressed: identification of snow and the choice of snow albedo.

The presence of snow in an OMI scene is currently determined using the Near-real-time Ice and Snow Extent (NISE; <http://nsidc.org/data/nise1.html>), an operational, daily, global product derived from the Special Sensor Microwave Imager/Sounder (SSMIS) passive microwave sensor (Nolin et al., 1998) on a 24 km × 24 km grid. When using an independent, ground-based determination of snow cover O'Byrne et al. (2010) found this product often missed thin snow cover, a common feature among snow products derived from passive microwave instruments. A similar evaluation was conducted here. Figure 4 shows comparisons (2000–2011) between daily snow cover from NISE compared with measurements made at two meteorological stations: Fort McMurray (30 km south of the surface mining) and Mildred Lake (in the middle of surface mining). When taking the surface-observed conditions as the truth, NISE misses snow cover roughly 30 % of the time in an annual average. Breaking this down by month (Fig. 4b) reveals

## Improved satellite retrievals of NO<sub>2</sub> and SO<sub>2</sub> over the Canadian oil sands

C. A. McLinden et al.

Title Page

Abstract

Introduction

Conclusions

References

Tables

Figures



Back

Close

Full Screen / Esc

Printer-friendly Version

Interactive Discussion







percent at most and so, on this basis, aerosols are neglected. An assessment of the uncertainty introduced from this assumption is provided in Sect. 4.1, below.

### 3.3 Calculation of AMFs

AMFs were calculated using the VECTOR (VECTor Orders-of-scattering Radiative transfer model) (McLinden et al., 2002, 2006; Wagner et al., 2007). As an initial step to verify the consistency between the AMFs computed using VECTOR to those provided in the DOMINO (v2.0) product, AMFs were calculated by VECTOR using the same input information as used by DOMINO, including the NO<sub>2</sub> profile, albedo, surface pressure, and geometry. For cloud-free pixels within 100 km of the reference location VECTOR AMFs were found to differ from the DOMINO AMFs on average by less than 3%. This agreement is acceptable given that not all input parameters were identical.

Using the input information described in Sect. 3.2, vertically-resolved AMFs,  $m(z)$ , were computed on a 0.5 km altitude grid between 0 and 16 km by successively perturbing the absorber over the 0.5 km layers and computing,

$$m(z) = -\frac{1}{I} \cdot \frac{\Delta I}{\Delta \tau(z)} \quad (5)$$

where  $\Delta I$  is the change in radiance for a change in the optical depth of  $\Delta \tau$  due to the perturbation. It is impractical to calculate  $m(z)$  for each OMI observation. Instead, a pair of multi-dimensional look-up tables for  $m(z)$ ,  $I$ , and  $f_{\text{dir}}$ , were generated, one for cloud-free conditions and one for cloudy conditions. Recall  $f_{\text{dir}}$  is used in the calculation of albedo in Eq. (3) and so is not relevant for cloud AMFs since the albedo is set to 0.8. The dependencies of the cloud-free table are surface albedo, solar zenith angle, viewing zenith angle, change in azimuthal angle, surface pressure, and column ozone. The dependencies of the cloud table are cloud-top pressure, solar zenith angle, viewing zenith angle, change in azimuthal angle, and column ozone. These are summarized in Table 2.

## Improved satellite retrievals of NO<sub>2</sub> and SO<sub>2</sub> over the Canadian oil sands

C. A. McLinden et al.

Title Page

Abstract

Introduction

Conclusions

References

Tables

Figures

⏪

⏩

◀

▶

Back

Close

Full Screen / Esc

Printer-friendly Version

Interactive Discussion





## 4.1 Error budget and sensitivity study

Beginning with Eq. (6), the total random uncertainty in VCD,  $\varepsilon$ , can be expressed as,

$$\varepsilon = \sqrt{\left(\frac{\varepsilon_s}{M}\right)^2 + \left(\frac{\varepsilon_{ss}}{M}\right)^2 + \left(\frac{\varepsilon_b}{M}\right)^2 + \left(V \cdot \frac{\varepsilon_M}{M}\right)^2} \quad (8)$$

where  $\varepsilon_i$  are uncertainties in the individual terms:  $\varepsilon_s$  is the uncertainty in the SCD,  $\varepsilon_{ss}$  in the stratospheric SCD,  $\varepsilon_b$  the SCD bias, and  $\varepsilon_M$  the AMF. Values for  $\varepsilon_s$  and  $\varepsilon_{ss}$  for  $\text{NO}_2$  are taken directly from Boersma et al. (2007) and  $\varepsilon_s$  for  $\text{SO}_2$  from Krokow et al. (2008). The uncertainty in the  $\text{SO}_2$  bias correction is based on the standard error of the mean of the bias, averaged over all months. These values are given in Table 3.

The uncertainty in AMF arises from several different sources, including uncertainties in cloud fraction, cloud pressure, surface albedo, profile shape, terrain height/surface pressure, aerosol, and stratospheric ozone. The impact of these on the AMF is assessed by varying each by an amount indicative of its own uncertainty and recalculating the AMF. For example, the surface albedo is varied by  $\pm 0.02$  and the extent to which this changes the AMF is taken as its uncertainty to this parameter. This is assessed using all OMI observations within 200 km of the reference location for the year 2005. Perturbing an input parameter in this way yields a distribution in the relative change in AMF. The standard deviation of the distribution is taken as the uncertainty to a given parameter and it is computed separately for polluted, within 50 km of the reference location, and background, between 50 and 200 km, areas. Only observations with radiative cloud fractions of 0.2 or smaller were considered. The results of this are also given in Table 3. The uncertainty due to profile shape was evaluated by recalculating AMFs but using profiles from GEOS-CHEM. Uncertainties in these parameters were assumed to be independent and so the total uncertainty in AMF was calculated by adding the individual terms in quadrature.

From Table 3 it can be seen that uncertainties in AMFs are about 20–25 % for  $\text{NO}_2$  and 25–35 % for  $\text{SO}_2$ , with the larger values for the polluted areas. In the case

### Improved satellite retrievals of $\text{NO}_2$ and $\text{SO}_2$ over the Canadian oil sands

C. A. McLinden et al.

Title Page

Abstract

Introduction

Conclusions

References

Tables

Figures



Back

Close

Full Screen / Esc

Printer-friendly Version

Interactive Discussion





## Improved satellite retrievals of NO<sub>2</sub> and SO<sub>2</sub> over the Canadian oil sands

C. A. McLinden et al.

Title Page

Abstract

Introduction

Conclusions

References

Tables

Figures

⏪

⏩

◀

▶

Back

Close

Full Screen / Esc

Printer-friendly Version

Interactive Discussion

tive of what might be expected from a doubling of emissions. Close to the source this led to an average reduction in AMF of 6%. Further away where there are no sources there should be little to no change. The relatively small impact suggests that a type of saturation effect is occurring: AMFs were already sufficiently weighted towards the PBL that adding additional NO<sub>2</sub> there had only a modest impact. Nonetheless, a 6% effect may still be an important when evaluating trends.

As discussed in Sect. 3.2.6, aerosols were not explicitly included in the AMF calculations. While difficult to uncouple from the aerosol-biased cloud fraction effect, this is a potential source of systematic error that needs to be explored. Similar to clouds, aerosols can either enhance the AMF due to increased scattering or decrease it by shielding an absorbing layer below. To assess this, AMFs were recalculated using single aerosol profile shape that decreases with altitude between 0 and 3 km, purely scattering, and scaled to give an optical depth of 0.1. The inclusion of aerosols acted to either increase or decrease AMF and is linked to the relative profile shapes and height of the PBL. On average aerosols decreased NO<sub>2</sub> AMF within the polluted area by 6%, with almost no impact over the background locations. Its average effect on SO<sub>2</sub> was about zero. A more comprehensive treatment would consider profiles shape what vary in space and time, and also take into account a correction for aerosols in the cloud retrieval.

### 4.2 VCD climatologies

Long-term (2005–2011) annual average NO<sub>2</sub> and SO<sub>2</sub> VCDs were calculated to examine their spatial distribution. Only small pixels (track positions 11–50), unaffected by the row-anomaly, snow-free, and observations with a radiative cloud fraction of 0.2 or less were considered here. In addition, SZAs were limited to 75° for NO<sub>2</sub> and 60° for SO<sub>2</sub>. Finally, SO<sub>2</sub> VCDs were restricted to values between –5 and +15 DU with the upper limit imposed to avoid spikes from volcanic eruptions. Averages were calculated using the oversampling, pixel averaging method of Fioletov et al. (2011) on a 1 km × 1 km grid

and with an averaging radius of 8 km for NO<sub>2</sub> and 24 km for SO<sub>2</sub>. The larger averaging radius for SO<sub>2</sub> is required due to its higher noise.

Averages are shown in Fig. 8 for the DOMINO and SP NO<sub>2</sub> and NASA SO<sub>2</sub> products. In each case, the corresponding maps based on EC-VCDs are also shown. The difference between the NO<sub>2</sub> EC-VCDs derived from the DOMINO and SP products lay mainly in how the stratosphere is removed. All maps show a clear enhancement over the region of surface mining consistent with the location of the largest emissions and in agreement with results from McLinden et al. (2012). The enhancement in NO<sub>2</sub> is largest over the southern mines but displays a secondary maximum over the northern cluster of mines whereas SO<sub>2</sub> is enhanced primarily only over the southern mines. This is also consistent with current information on source locations: SO<sub>2</sub> is emitted principally from upgrading facilities (which convert bitumen to synthetic crude) in the south whereas NO<sub>2</sub> also has area sources from transportation (e.g., the heavy-hauler trucks) in both the north and south. Despite the more diffuse source of NO<sub>2</sub>, the SO<sub>2</sub> enhancement is seen to cover a larger area. This is suggestive of a longer lifetime. Also worth noting is the difference in the height of the release: much of the NO<sub>x</sub> is emitted at the surface (transportation) whereas SO<sub>2</sub> is emitted primarily from stacks some 200–300 m above the surface where winds are generally faster.

The DOMINO (Fig. 8a) and NASA SP (Fig. 8c) NO<sub>2</sub> are generally consistent with SP being 30 % larger over the mines. The difference between DOMINO and EC (Fig. 8b) NO<sub>2</sub> are consistent with what might have been expected from the AMFs: comparable spatial distributions with similar background values but over the surface mines the EC VCDs are larger by a factor of up to 1.9. The same is true when comparing the NASA (Fig. 8e) and EC (Fig. 8f) SO<sub>2</sub>, with the EC larger by up to a factor of 1.3. Note that the EC-VCDs derived from the DOMINO (Fig. 8b) and SP (Fig. 8d) products are in very good agreement, differences are less than 10 % over the mines and about  $2 \times 10^{14} \text{ cm}^{-2}$  in the background.

The mass of these enhancements, where the enhancement is defined as the NO<sub>2</sub> or SO<sub>2</sub> above the background (presumably from oil sands operations), was determined by

## Improved satellite retrievals of NO<sub>2</sub> and SO<sub>2</sub> over the Canadian oil sands

C. A. McLinden et al.

Title Page

Abstract

Introduction

Conclusions

References

Tables

Figures

⏪

⏩

◀

▶

Back

Close

Full Screen / Esc

Printer-friendly Version

Interactive Discussion





## Improved satellite retrievals of NO<sub>2</sub> and SO<sub>2</sub> over the Canadian oil sands

C. A. McLinden et al.

Title Page

Abstract

Introduction

Conclusions

References

Tables

Figures

◀

▶

◀

▶

Back

Close

Full Screen / Esc

Printer-friendly Version

Interactive Discussion

to all wind directions. This approach is favoured as satellites measure over a large area (~ 500 km<sup>2</sup> for OMI) and weight the upwind and downwind directions equally. Averaging in this way, as opposed to a “simple” average that preferentially weights the prevailing wind direction, impacts the mean NO<sub>2</sub> values by between –15 % to +15 %. For SO<sub>2</sub> the effect is larger, –30 % to +30 %, which reflects its more localized sources.

One additional effect was considered in advance of the GB-satellite comparisons. The GB NO<sub>2</sub> measurements are made by commercial, chemiluminescence analyzers that rely on molybdenum converters. These instruments alternate between measuring NO<sub>x</sub> and NO, with NO<sub>2</sub> inferred as the difference. However, it is well known that these instruments are also sensitive to nitric acid, peroxyacetyl nitrate (PAN), and other oxidized nitrogen-containing species (Winer et al., 1974; Lamsal et al., 2008) which are mistakenly interpreted as NO<sub>2</sub>. A simple factor, CF, for this “interference” effect was used herein, following Lamsal et al. (2008, 2010),

$$CF = \frac{NO_2}{NO_2 + \sum AN + 0.15 \cdot HNO_3 + 0.95 \cdot PAN} \quad (10)$$

and based on model calculated concentrations (ΣAN is the sum of all alkyl nitrates and PAN is peroxyacetyl nitrate). The multipliers preceding PAN and HNO<sub>3</sub> account for the reduced conversion efficiency of these species by the instrument. Equation (4) was evaluated separately for monthly-mean GEM-MACH and GEOS-CHEM concentrations and their average CF was used to correct the GB measurements. At the relatively low NO<sub>2</sub> levels over the oil sands (average values of < 5 ppb) this correction factor can be considerably smaller than one due to the larger contribution of non-NO<sub>x</sub> oxygenated nitrogen species (Lamsal et al., 2008). The station-specific correction factors are given in Table S1. Values range from 0.35 to 0.7, with the smaller factors corresponding to smaller mean NO<sub>2</sub> levels. It is difficult to determine the accuracy of these correction factors and errors due to both the modelled species concentration ratios and the conversion efficiencies (which can vary from instrument-to-instrument) may be appre-

5 ciable. For simplicity, in this work the difference between the two model evaluations of CF was used as a measure of its uncertainty.

From Figs. 11 and 12, the EC-vmrs are able to capture the spatial variation and gradients of the NO<sub>2</sub> and SO<sub>2</sub> displayed by the GB stations through the mining region. For NO<sub>2</sub> (Fig. 11), the EC-vmrs are typically smaller than the GB values (with the CF applied) by a factor of two (roughly 1 ppb) with the exception of the Millennium station (#3), where the differences are larger (3 ppb, a factor of 5). There is no obvious explanation for the larger differences in NO<sub>2</sub> at Millennium and the measurements are roughly constant with wind direction. Excluding Millennium, the slope of the scatterplot is 0.54 and the correlation coefficient is 0.80. The SO<sub>2</sub> comparison (Fig. 12) shows much better agreement including the Millennium station (slope of 0.88; correlation coefficient of 0.91). A summary of the linear correlation coefficients and slopes are given in Table 4.

Given its spatial resolution, OMI is only able to provide a smoothed version of the true surface vmr distribution. Indeed, this may be the origin of some of the GB-satellite differences seen in Figs. 11 and 12. To better understand this, idealized estimates of the true NO<sub>2</sub> and SO<sub>2</sub> surface vmr distributions were constructed assuming the distribution resulting from a source “region” is reasonably represented by a 2-D gaussian. Parameters for the gaussians were selected so that (i) their vmrs were comparable to the average measured values at the GB stations and (ii) after smoothing the distributions generally resembled those from Fig. 8 (although not necessarily the absolute values). For NO<sub>2</sub>, the sum of three Gaussians was used: one each for the north and south grouping of mines, and a smaller one for the Fort McMurray area. For SO<sub>2</sub> only one Gaussian was used, reflecting the lack of a significant source of SO<sub>2</sub> in the north or Fort McMurray. GB measurements from Fort Chipewyan (station 12) were used to define background values. These idealized distributions were then smoothed using a 15 km × 30 km 2-D boxcar to simulate the OMI pixel size, and both original and smoothed distributions (shown in the Supplement) were sampled at the location of the WBEA stations using values with 6 km for NO<sub>2</sub> or 12 km for SO<sub>2</sub>. As expected, stations

**Improved satellite retrievals of NO<sub>2</sub> and SO<sub>2</sub> over the Canadian oil sands**

C. A. McLinden et al.

Title Page

Abstract

Introduction

Conclusions

References

Tables

Figures



Back

Close

Full Screen / Esc

Printer-friendly Version

Interactive Discussion



near the peaks became smaller and those in the wings became larger as a result of the smoothing: NO<sub>2</sub> was impacted by -35% to +15%, SO<sub>2</sub> by -10 to +30%. Of particular note is NO<sub>2</sub> is near stations 8 and 9 which suggest that there is a local minimum between the two mining regions (see also Fig. 11).

Ignored to this point is the clear-sky bias in the OMI measurements resulting from the requirement that only (near) cloud-free measurements be used, with no such restriction on the GB measurements. Averaging over clear-sky data only may introduce a bias from the direct effect of generally faster photochemistry due to higher levels of sunlight, including the photolysis rate of NO<sub>2</sub> which is important in the NO-NO<sub>2</sub> partitioning. There may also be an indirect effect if cloudiness is correlated with wind direction, and hence air mass origin. The most obvious way of avoiding this bias is to sample the GB data in the same way as OMI. However, this is complicated by the method used here to compute GB station averages: first calculating averages as a function of wind direction, and then averaging over these. Another method of removing clear-sky bias is to use a measure of cloud cover at each of surface stations to screen GB measurements, analogous to the satellite measurements, with the source of cloud information being either a surface monitor or the OMI or MODIS-Aqua cloud fraction products (e.g., Geddes et al., 2012). A third alternative, and the approach used here, is to compare NO<sub>2</sub> and SO<sub>2</sub> from GEM-MACH with and without cloud-screening. Limiting NO<sub>2</sub> to clear-skies leads to a low bias, relative to all-sky conditions, in an amount varying from 5–50%. This is similar to the clear-sky bias observed over the greater Toronto area (Geddes et al., 2012) and consistent with a shift in the NO<sub>x</sub> partitioning to favour NO as a result of increased photolysis. For SO<sub>2</sub> the opposite effect was observed: cloud screening led to a high bias between 5 and 25%. Scavenging of SO<sub>2</sub> by clouds is an efficient loss mechanism, thus higher SO<sub>2</sub> concentrations when considering only cloud-free conditions are expected. Average clear-sky biases are given in the Supplement.

The impact of smoothing and clear-sky bias on the GB-satellite comparison was assessed by applying the scaling factors for each to the EC-vmrs. These are also shown in Figs. 11 and 12, and the linear corrections and slopes are given in Table 4.

## Improved satellite retrievals of NO<sub>2</sub> and SO<sub>2</sub> over the Canadian oil sands

C. A. McLinden et al.

Title Page

Abstract

Introduction

Conclusions

References

Tables

Figures

⏪

⏩

◀

▶

Back

Close

Full Screen / Esc

Printer-friendly Version

Interactive Discussion



## Improved satellite retrievals of NO<sub>2</sub> and SO<sub>2</sub> over the Canadian oil sands

C. A. McLinden et al.

Title Page

Abstract

Introduction

Conclusions

References

Tables

Figures

⏪

⏩

◀

▶

Back

Close

Full Screen / Esc

Printer-friendly Version

Interactive Discussion

The EC-VMR NO<sub>2</sub> increased at all stations and substantially improved the agreement. Excluding Millennium, which showed almost no change, now gives a scatter-plot slope of 0.65 and a correlation coefficient of 0.91. Also of note is the ability of the EC-vmrs to capture the minimum in NO<sub>2</sub> between the northern and southern mining regions. In contrast, there was a smaller impact on SO<sub>2</sub> as the two effects somewhat cancelled (slope 1.01; correlation coefficient 0.91). The combined effect of the smoothing and clear-sky bias corrections explains (with the exception of Millennium) a large portion of the GB-satellite difference in NO<sub>2</sub> and highlights its importance.

To conclude this section, it is noted that the stringent SZA threshold of 60° (combined with the snow filter) means > 99 % of OMI SO<sub>2</sub> measurements considered are from April to September. For NO<sub>2</sub>, with a SZA threshold of 75°, the breakdown is about 75 % (April–September): 25 % (October–March) which allows for some seasonal analysis. The comparison above was repeated but for limited to these two 6 month “seasons”. For April–September, the agreement between GB and EC-vmrs improved (slope 1.00, correlation coefficient 0.94) and October–March the agreement decreased (slope 0.47, correlation coefficient 0.68). The relative poor agreement in winter could simply be due to larger SZAs or a result of the shallower BL heights in the winter. Part of the underestimate by the EC-vmrs could be related to the simplified treatment of surface reflection. Zhou et al. (2010) predict a 10–20 % underestimate in the winter when using the surface is modelled as a Lambertian reflector instead of the more rigorous BRDF. A more detailed investigation into these differences is beyond the scope of this study.

## 6 Summary and conclusions

Significant low biases have been identified in current NO<sub>2</sub> and SO<sub>2</sub> retrieval products from the Ozone Monitoring instrument (OMI) over the Canadian oil sands arising from a combination of its rapid development and small spatial scale. Air mass factors (AMFs) were re-calculated for this region based on updated and higher resolution input information. These include: gas absorber profiles from the high-resolution (15 km × 15 km)

GEM-MACH air quality forecast model, higher spatial and temporal resolution surface reflectivity from the MODIS satellite instruments, and an improved treatment of snow via a more precise determination of snow cover and more appropriate surface albedo when snow is present.

5 The overall impact of these new Environment Canada AMFs led to increases in the peak NO<sub>2</sub> and SO<sub>2</sub> average vertical column density (VCD), occurring over the area of intensive surface mining, by factors of roughly 2 and 1.5, respectively. Due to a lack of validation profile or VCD data in this region, comparisons were made with long-term averages of NO<sub>2</sub> and SO<sub>2</sub> from in-situ surface monitors at several WBEA stations. This was achieved by using the AQ model to map the EC-VMR VCDs to surface concentrations. The OMI-EC surface concentrations were able to capture the NO<sub>2</sub> and SO<sub>2</sub> spatial distribution of the in-situ instruments. The absolute values were in reasonable agreement with OMI-EC surface NO<sub>2</sub> and SO<sub>2</sub> biased low by roughly 30 %. The exception to this is the NO<sub>2</sub> comparison at the Millenium monitoring station which showed much larger values. This level of agreement was improved by addressing complications in these comparisons. The first was the NO<sub>2</sub> high bias in the molybdenum-based surface instruments. The other two were the effects of smoothing by OMI and the clear-sky bias.

20 This work is the first attempt to homogenize the OMI NO<sub>2</sub> and SO<sub>2</sub> data products through a consistent treatment of AMFs. It also examines the impact of inter-annual variability in a number of AMF-dependent parameters including profile shape, surface albedo, and ozone column. The use of output from the high-resolution air quality model GEM-MACH was valuable in several regards: input into the AMF calculations, for performing the column to surface mapping, and also in assessing the sources of bias. Overall these results highlight the importance of using input information that accounts for the spatial and temporal variability at the location of interest when performing retrievals.

Improved satellite retrievals of NO<sub>2</sub> and SO<sub>2</sub> over the Canadian oil sands

C. A. McLinden et al.

Title Page

Abstract Introduction

Conclusions References

Tables Figures

⏪ ⏩

◀ ▶

Back Close

Full Screen / Esc

Printer-friendly Version

Interactive Discussion



Supplementary material related to this article is available online at  
[http://www.atmos-chem-phys-discuss.net/13/21609/2013/  
acpd-13-21609-2013-supplement.pdf](http://www.atmos-chem-phys-discuss.net/13/21609/2013/acpd-13-21609-2013-supplement.pdf).

*Acknowledgements.* The authors thank the Wood Buffalo Environmental Association (WBEA) for the provision of their in-situ data. We acknowledge the free use of tropospheric NO<sub>2</sub> column data from the OMI sensor from [www.temis.nl](http://www.temis.nl). We also acknowledge the NASA Earth Science Division for funding of OMI NO<sub>2</sub> and SO<sub>2</sub> products development and analysis.

## References

- Anselmo, D., Moran, M. D., Menard, S., Bouchet, V., Makar, P., Gong, W., Kallaur, A., Beaulieu, P.-A., Landry, H., Stroud, C., Huang, P., Gong, S., and Talbot, D.: A new Canadian air quality forecast model: GEM-MACH15, Proc. 12th AMS Conf. on Atmos. Chem, 17–21 January, Atlanta, Ga, American Meteorological Society, Boston, MA., 6 pp., 2010, available at: <http://ams.confex.com/ams/pdfpapers/165388.pdf>, last access 8 August 2013.
- Beirle, S., Boersma, K. F., Platt, U., Lawrence, M. G., and Wagner, T.: Megacity emissions and lifetimes of nitrogen oxides probed from space, *Science*, 333, 1737–1739, 2011.
- Bey, I., Jacob, D. J., Yantosca, R. M., Logan, J. A., Field, B., Fiore, A. M., Li, Q., Liu, H., Mickley, L. J., and Schultz, M.: Global modeling of tropospheric chemistry with assimilated meteorology: model description and evaluation, *J. Geophys. Res.*, 106, 23073–23096, 2001.
- Boersma, K. F., Eskes, H. J., and Brinksma, E. J.: Error analysis for tropospheric NO<sub>2</sub> retrieval from space, *J. Geophys. Res.*, 109, D04311, doi:10.1029/2003JD003962, 2004.
- Boersma, K. F., Eskes, H. J., Veefkind, J. P., Brinksma, E. J., van der A, R. J., Sneep, M., van den Oord, G. H. J., Levelt, P. F., Stammes, P., Gleason, J. F., and Bucsela, E. J.: Near-real time retrieval of tropospheric NO<sub>2</sub> from OMI, *Atmos. Chem. Phys.*, 7, 2103–2118, doi:10.5194/acp-7-2103-2007, 2007.
- Boersma, K. F., Jacob, D. J., Trainic, M., Rudich, Y., DeSmedt, I., Dirksen, R., and Eskes, H. J.: Validation of urban NO<sub>2</sub> concentrations and their diurnal and seasonal variations observed from the SCIAMACHY and OMI sensors using in situ surface measurements in Israeli cities, *Atmos. Chem. Phys.*, 9, 3867–3879, doi:10.5194/acp-9-3867-2009, 2009.

## Improved satellite retrievals of NO<sub>2</sub> and SO<sub>2</sub> over the Canadian oil sands

C. A. McLinden et al.

Title Page

Abstract

Introduction

Conclusions

References

Tables

Figures

⏪

⏩

◀

▶

Back

Close

Full Screen / Esc

Printer-friendly Version

Interactive Discussion



## Improved satellite retrievals of NO<sub>2</sub> and SO<sub>2</sub> over the Canadian oil sands

C. A. McLinden et al.

Title Page

Abstract

Introduction

Conclusions

References

Tables

Figures

⏪

⏩

◀

▶

Back

Close

Full Screen / Esc

Printer-friendly Version

Interactive Discussion

- Boersma, K. F., Eskes, H. J., Dirksen, R. J., van der A, R. J., Veefkind, J. P., Stammes, P., Huijnen, V., Kleipool, Q. L., Sneep, M., Claas, J., Leitão, J., Richter, A., Zhou, Y., and Brunner, D.: An improved tropospheric NO<sub>2</sub> column retrieval algorithm for the Ozone Monitoring Instrument, *Atmos. Meas. Tech.*, 4, 1905–1928, doi:10.5194/amt-4-1905-2011, 2011.
- 5 Bovensmann, H., Burrows, J. P., Buchwitz, M., Frerick, J., Noël, S., Rozanov, V. V., Chance, K. V., and Goede, A. P. H.: SCIAMACHY: Mission Objectives and Measurement Modes, *J. Atmos. Sci.*, 56, 127–150, doi:10.1175/1520-0469(1999)056<0127:SMOAMM>2.0.CO;2, 1999.
- Brown, R. D., Brasnett, B., and Robinson, D.: Gridded North American monthly snow depth and snow water equivalent for GCM evaluation, *Atmos.-Ocean*, 41, 1–14, doi:10.3137/ao.4110101, 2003.
- 10 Burrows, J. P., Weber, M., Buchwitz, M., Rozanov, V., Ladstätter-Weissenmayer, A., Richter, A., DeBeek, R., Hoogen, R., Bramstedt, K., Eichmann, K. U., Eisinger, M., and Perner, D.: The global ozone monitoring experiment (GOME): Mission concept and first scientific results, *J. Atmos. Sci.*, 56, 151–175, 1999.
- 15 Bucsela, E. J., Krotkov, N. A., Celarier, E. A., Lamsal, L. N., Swartz, W. H., Bhartia, P. K., Boersma, K. F., Veefkind, J. P., Gleason, J. F., and Pickering, K. E.: A new stratospheric and tropospheric NO<sub>2</sub> retrieval algorithm for nadir-viewing satellite instruments: applications to OMI, *Atmos. Meas. Tech. Discuss.*, 6, 1361–1407, doi:10.5194/amtd-6-1361-2013, 2013.
- 20 Chen, D., Wang, Y., McElroy, M. B., He, K., Yantosca, R. M., and Le Sager, P.: Regional CO pollution and export in China simulated by the high-resolution nested-grid GEOS-Chem model, *Atmos. Chem. Phys.*, 9, 3825–3839, doi:10.5194/acp-9-3825-2009, 2009.
- Côté, J., Gravel, S., Méthot, A., Patoine, A., Roch, M., and Staniforth, A.: The operational CMC-MRB Global Environmental Multiscale (GEM) model. Part 1: Design considerations and formulation, *Mon. Weather Rev.*, 126, 1373–1395, 1998.
- 25 Dirksen, R. J., Boersma, K. F., Eskes, H. J., Ionov, D. V., Bucsela, E. J., Levelt, P. F., and Kelder, H. M.: Evaluation of stratospheric NO<sub>2</sub> retrieved from the Ozone Monitoring Instrument: intercomparison, diurnal cycle and trending, *J. Geophys. Res.*, 116, D08305, doi:10.1029/2010JD014943, 2011.
- 30 ERCB (Energy Resources Conservation Board) (2012), ST98:2012: Alberta's Energy Resources 2011 and Supply/Demand Outlook 2012–2021, Calgary, Alberta: Energy Resources Conservation Board, available at: <http://www.ercb.ca/>, last access 8 August 2013.

## Improved satellite retrievals of NO<sub>2</sub> and SO<sub>2</sub> over the Canadian oil sands

C. A. McLinden et al.

Title Page

Abstract

Introduction

Conclusions

References

Tables

Figures

◀

▶

◀

▶

Back

Close

Full Screen / Esc

Printer-friendly Version

Interactive Discussion

- Fioletov, V. E., McLinden, C. A., Krotkov, N., Moran, M. D., and Yang, K.: Estimation of SO<sub>2</sub> emissions using OMI retrievals, *Geophys. Res. Lett.*, **38**, L21811, doi:10.1029/2011GL049402, 2011.
- 5 Fioletov, V. E., McLinden, C. A., Krotkov, N., Yang, K., Loyola, D. G., Valks, P., Theys, N., Van Roozendaal, M., Nowlan, C., Chance, K., Liu, X., Lee, C., and Martin, R. V.: Application of OMI, SCIAMACHY and GOME-2 satellite SO<sub>2</sub> retrievals for detection of large emission sources, *J. Geophys. Res.*, doi:10.1029/2013JD019967, in review, 2013.
- Frei, A. and Lee, S.: A comparison of optical-band based snow extent products during spring over North America, *Remote Sens. Environ.*, **114**, 1940–1948, 2010.
- 10 Gao, F., Schaaf, C. B., Strahler, A. H., Roesch, A., Lucht, W., and Dickinson, R.: MODIS bidirectional reflectance distribution function and albedo Climate Modeling Grid products and the variability of albedo for major global vegetation types, *J. Geophys. Res.*, **110**, D01104, doi:10.1029/2004JD005190, 2005.
- 15 Geddes, J. A., Murphy, J. G., O'Brien, J. M., and Celarier, E. A.: Biases in long-term NO<sub>2</sub> averages inferred from satellite observations due to cloud selection criteria, *Remote Sens. Env.*, **124**, 210–216, 2012.
- Gong, W., Dastoor, A. P., Bouchet, V. S., Gong, S. L., Makar, P. A., Moran, M. D., Pabla, B., Menard, S., Crevier, L.-P., Cousineau, S., and Venkatesh, S.: Cloud processing of gases and aerosols in a regional air quality model (AURAMS), *Atmos. Res.*, **82**, 248–275, 2006.
- 20 Heckel, A., Kim, S.-W., Frost, G. J., Richter, A., Trainer, M., and Burrows, J. P.: Influence of low spatial resolution a priori data on tropospheric NO<sub>2</sub> satellite retrievals, *Atmos. Meas. Tech.*, **4**, 1805–1820, doi:10.5194/amt-4-1805-2011, 2011.
- Helfrich, S. R., McNamara, D., Ramsay, B. H., Baldwin, T., and Kasheta, T.: Enhancements to, and forthcoming developments in the Interactive Multisensor Snow and Ice Mapping System (IMS), *Hydrol. Process.*, **21**, 1576–1586, doi:10.1002/HYP.6720, 2007.
- 25 Hudman, R. C., Jacob, D. J., Turquety, S., Leibensperger, E. M., Murray, L. T., Wu, S., Gilliland, A. B., Avery, M., Bertram, T. H., Brune, W., Cohen, R. C., Dibb, J. E., Flocke, F. M., Fried, A., Holloway, J., Neuman, J. A., Orville, R., Perring, A., Ren, X., Sachse, G. W., Singh, H. B., Swanson, A., and Wooldridge, P. J.: Surface and lightning sources of nitrogen oxides over the United States: magnitudes, chemical evolution, and outflow, *J. Geophys. Res.*, **112**, D12S05, doi:10.1029/2006JD007912, 2007.
- 30 Kukkonen, J., Olsson, T., Schultz, D. M., Baklanov, A., Klein, T., Miranda, A. I., Monteiro, A., Hirtl, M., Tarvainen, V., Boy, M., Peuch, V.-H., Poupkou, A., Kioutsioukis, I., Finardi, S.,

**Improved satellite retrievals of NO<sub>2</sub> and SO<sub>2</sub> over the Canadian oil sands**

C. A. McLinden et al.

Title Page

Abstract

Introduction

Conclusions

References

Tables

Figures

⏪

⏩

◀

▶

Back

Close

Full Screen / Esc

Printer-friendly Version

Interactive Discussion

Sofiev, M., Sokhi, R., Lehtinen, K. E. J., Karatzas, K., San José, R., Astitha, M., Kallos, G., Schaap, M., Reimer, E., Jakobs, H., and Eben, K.: A review of operational, regional-scale, chemical weather forecasting models in Europe, *Atmos. Chem. Phys.*, 12, 1–87, doi:10.5194/acp-12-1-2012, 2012.

5 Kleipool, Q. L., Dobber, M. R., de Haan, J. F., and Levelt, P. F.: Earth surface reflectance climatology from 3 years of OMI data, *J. Geophys. Res.*, 113, D18308, doi:10.1029/2008JD010290, 2008.

Krotkov, N. A., Carn, S. A., Krueger, A. J., Bhartia, P. K., and Yang, K.: Band residual difference algorithm for retrieval of SO<sub>2</sub> from the Aura Ozone Monitoring Instrument (OMI), *IEEE Trans. Geosci. Remote Sens.*, 44, 1259–1266, doi:10.1109/TGRS.2005.861932, 2006.

10 Krotkov, N. A., McClure, B., Dickerson, R. R., Carn, S. A., Li, C., Bhartia, P. K., Yang, K., Krueger, A. J., Li, Z., Levelt, P. F., Chen, H., Wang, P., and Lu, D.: Validation of SO<sub>2</sub> retrievals from the Ozone Monitoring Instrument (OMI) over NE China, *J. Geophys. Res.*, 113, D16S40, doi:10.1029/2007JD008818, 2008.

15 Lamsal, L. N., Martin, R. V., van Donkelaar, A., Steinbacher, M., Celarier, E. A., Bucsela, E., Dunlea, E. J., and Pinto, J. P.: Ground-level nitrogen dioxide concentrations inferred from the satellite-borne Ozone Monitoring Instrument, *J. Geophys. Res.*, 113, D16308, doi:10.1029/2007JD009235, 2008.

20 Lamsal, L. N., Martin, R. V., van Donkelaar, A., Celarier, E. A., Bucsela, E. J., Boersma, K. F., Dirksen, R., Luo, C., and Wang, Y.: Indirect validation of tropospheric nitrogen dioxide retrieved from the OMI satellite instrument: Insight into the seasonal variation of nitrogen oxides at northern midlatitudes, *J. Geophys. Res.*, 115, D05302, doi:10.1029/2009JD013351, 2010.

25 Lee, C., Martin, R. V., van Donkelaar, A., O’Byrne, G., Krotkov, N., Richter, A., Huey, L. G., and Holloway, J. S.: Retrieval of vertical columns of sulfur dioxide from SCIAMACHY and OMI: air mass factor algorithm development, validation, and error analysis, *J. Geophys. Res.*, 114, D22303, doi:10.1029/2009JD012123, 2009.

Levelt, P. F., van den Oord, G. H. J., Dobber, M. R., Mälkki, A., Visser, H., de Vries, J., Stammes, P., Lundell, J. O. V., and Saari, H.: The ozone monitoring instrument, *IEEE Trans. Geosci. Remote Sens.*, 44, 1093–1101, 2006.

30 Martin, R. V.: Satellite remote sensing of surface air quality, *Atmos. Environ.*, 42, 7823–7843, 2008.

## Improved satellite retrievals of NO<sub>2</sub> and SO<sub>2</sub> over the Canadian oil sands

C. A. McLinden et al.

Title Page

Abstract

Introduction

Conclusions

References

Tables

Figures

⏪

⏩

◀

▶

Back

Close

Full Screen / Esc

Printer-friendly Version

Interactive Discussion



Martin, R. V., Chance, K., Jacob, D. J., Kurosu, T. P., Spurr, R. J. D., Bucsela, E., Gleason, J. F., Palmer, P. I., Bey, I., Fiore, A. M., Li, Q., Yantosca, R. M., and Koelemeijer, R. B. A.: An improved retrieval of tropospheric nitrogen dioxide from GOME, *J. Geophys. Res.*, 107, 4437, doi:10.1029/2001JD001027, 2002.

5 Martin, R. V., Jacob, D. J., Chance, K. V., Kurosu, T. P., Palmer, P. I., and Evans, M. J.: Global inventory of nitrogen dioxide emissions constrained by space-based observations of NO<sub>2</sub> columns, *J. Geophys. Res.*, 108, 4537, doi:10.1029/2003/JD003453, 2003.

Martin, R. V., Sioris, C. E., Chance, K., Ryerson, T. B., Bertram, T. H., Wooldridge, P. J., Cohen, R. C., Neuman, J. A., Swanson, A., and Flocke, F. M.: Evaluation of space-based constraints on global nitrogen oxide emissions with regional aircraft measurements over and downwind of eastern North America, *J. Geophys. Res.*, 111, D15308, doi:10.1029/2005JD006680, 2006.

Martin, R. V., Sauvage, B., Folkins, I., Sioris, C. E., Boone, C., Bernath, P., and Ziemke, J.: Space-based constraints on the production of nitric oxide by lightning, *J. Geophys. Res.*, 112, D09309, doi:10.1029/2006JD007831, 2007.

15 McLinden, C. A., McConnell, J. C., Griffioen, E., and McElroy, C. T.: A vector radiative transfer model for the Odin/OSIRIS project, *Can. J. Phys.*, 80, 375–393, 2002.

McLinden, C. A., Haley, C. S., and Sioris, C. E.: Diurnal effects in limb scatter observations, *J. Geophys. Res.*, 111, D14302, doi:10.1029/2005JD006628, 2006.

20 McLinden, C. A., Fioletov, V., Boersma, K. F., Krotkov, N., Sioris, C. E., Veefkind, J. P., and Yang, K.: Air quality over the Canadian oil sands: a first assessment using satellite observations, *Geophys. Res. Lett.*, 39, L04804, doi:10.1029/2011GL050273, 2012.

Miyazaki, K., Eskes, H. J., and Sudo, K.: Global NO<sub>x</sub> emission estimates derived from an assimilation of OMI tropospheric NO<sub>2</sub> columns, *Atmos. Chem. Phys.*, 12, 2263–2288, doi:10.5194/acp-12-2263-2012, 2012.

25 Moody, E. G., King, M. D., Schaaf, C. B., Hall, D. K., and Platnick, S.: Northern Hemisphere five-year average (2000–2004) spectral albedos of surfaces in the presence of snow: statistics computed from Terra MODIS land products, *Remote Sens. Environ.*, 111, 337–345, doi:10.1016/j.rse.2007.03.026, 2007.

30 Moran, M. D., Menard, S., Talbot, D., Huang, P., Makar, P. A., Gong, W., Landry, H., Gong, S., Gravel, S., Crevier, L.-P., and Kallaur, A.: Particulate-matter forecasting with GEM-MACH15, a new Canadian operational air quality forecast model, Proc. 30th NATO/SPS ITM on Air Pollution Modelling and its Application, San Francisco, 18–22 May, 4 pp., published as Air

## Improved satellite retrievals of NO<sub>2</sub> and SO<sub>2</sub> over the Canadian oil sands

C. A. McLinden et al.

Title Page

Abstract

Introduction

Conclusions

References

Tables

Figures

⏪

⏩

◀

▶

Back

Close

Full Screen / Esc

Printer-friendly Version

Interactive Discussion

Pollution Modelling and its Application XX, 2010, edited by: Steyn, D. G. and Rao, S. T., Springer, Dordrecht, 289–293, 2009.

Nolin, A., Armstrong, R. L., and Maslanik, J.: Near-Real-Time SSM/I EASE-Grid Daily Global Ice Concentration and Snow Extent (2004–present), digital media, Natl. Snow and Ice Data Cent., Boulder, CO, 1998.

O’Byrne, G., Martin, R. V., van Donkelaar, A., Joiner, J., and Celarier, E. A.: Surface reflectivity from OMI using MODIS to eliminate clouds: effects of snow on UV-Vis trace gas retrievals, *J. Geophys. Res.*, 115, D17305, doi:10.1029/2009JD013079, 2010.

Palmer, P. I., Jacob, D. J., Chance, K., Martin, R. V., Spurr, R. J. D., Kurosu, T. P., Bey, I., Yantosca, R., Fiore, A., and Li, Q.: Air mass factor formulation for spectroscopic measurements from satellites: application to formaldehyde retrievals from the Global Ozone Monitoring Experiment, *J. Geophys. Res.*, 106, 14539–14550, 2001.

Park, R. J., Jacob, D. J., Field, B. D., Yantosca, R. M., and Chin, M.: Natural and transboundary pollution influences on sulfate-nitrate-ammonium aerosols in the United States: implications for policy, *J. Geophys. Res.*, 109, D15204, doi:10.1029/2003JD004473, 2004,

Percy, K. E., Hansen, M. C., and Dann, T.: Air Quality in the Athabasca Oil Sands Region, in: Volume 11: Alberta Oil Sands, Energy, Industry and the Environment, edited by: Percy, K., Elsevier, Amsterdam, the Netherlands, 2012.

Platt, U.: Differential optical absorption spectroscopy (DOAS), in: Air Monitoring by Spectroscopic Techniques, edited by: Sigrist, M., John Wiley, Hoboken, NJ, 27–84, 1994.

Russell, A. R., Perring, A. E., Valin, L. C., Bucsela, E. J., Browne, E. C., Wooldridge, P. J., and Cohen, R. C.: A high spatial resolution retrieval of NO<sub>2</sub> column densities from OMI: method and evaluation, *Atmos. Chem. Phys.*, 11, 8543–8554, doi:10.5194/acp-11-8543-2011, 2011.

Sauvage, B., Martin, R. V., van Donkelaar, A., Liu, X., Chance, K., Jaeglé, L., Palmer, P. I., Wu, S., and Fu, T.-M.: Remote sensed and in situ constraints on processes affecting tropical tropospheric ozone, *Atmos. Chem. Phys.*, 7, 815–838, doi:10.5194/acp-7-815-2007, 2007.

Schaaf, C. B., Gao, F., Strahler, A. H., Lucht, W., Li, X., Tsang, T., Strugnell, N. C., Zhang, X., Jin, Y., Muller, J.-P., Lewis, P., Barnsley, M., Hobson, P., Disney, M., Roberts, G., Dunderdale, M., Doll, C., d’Entremont, R. P., Hu, B., Liang, S., Privette, J. L., and Roy, D.: First operational BRDF, albedo nadir reflectance products from MODIS, *Remote Sens. Environ.*, 83, 135–148, 2002.

Streets, D. G., Canty, T., Carmichael, G. R., de Foy, B., Dickerson, R. R., Duncan, B. N., Edwards, D. P., Haynes, J. A., Henze, D. K., Houyoux, M. R., Jacob, D. J., Krotkov, N. A.,

**Improved satellite retrievals of NO<sub>2</sub> and SO<sub>2</sub> over the Canadian oil sands**

C. A. McLinden et al.

[Title Page](#)[Abstract](#)[Introduction](#)[Conclusions](#)[References](#)[Tables](#)[Figures](#)[⏪](#)[⏩](#)[◀](#)[▶](#)[Back](#)[Close](#)[Full Screen / Esc](#)[Printer-friendly Version](#)[Interactive Discussion](#)

Lamsal, L. N., Liu, Y., Lu, Z., Martin, R. V., Pfister, G. G., Pinder, R. W., Salawitch, R. J., and Wecht, K. J.: Emissions estimation from satellite retrievals: a review of current capability, *Atmos. Environ.*, 77, 1011–1042, doi:10.1016/j.atmosenv.2013.05.051, 2013.

Wagner, T., Burrows, J. P., Deutschmann, T., Dix, B., von Friedeburg, C., Frieß, U., Hendrick, F., Heue, K.-P., Irie, H., Iwabuchi, H., Kanaya, Y., Keller, J., McLinden, C. A., Oetjen, H., Palazzi, E., Petritoli, A., Platt, U., Postlyakov, O., Pukite, J., Richter, A., van Roozendael, M., Rozanov, A., Rozanov, V., Sinreich, R., Sanghavi, S., and Wittrock, F.: Comparison of box-air-mass-factors and radiances for Multiple-Axis Differential Optical Absorption Spectroscopy (MAX-DOAS) geometries calculated from different UV/visible radiative transfer models, *Atmos. Chem. Phys.*, 7, 1809–1833, doi:10.5194/acp-7-1809-2007, 2007.

Wenig, M. O., Cede, A. M., Bucsela, E. J., Celarier, E. A., Boersma, K. F., Veefkind, J. P., Brinksma, E. J., Gleason, J. F., and Herman, J. R.: Validation of OMI tropospheric NO<sub>2</sub> column densities using direct-Sun mode Brewer measurements at NASA Goddard Space Flight Center, *J. Geophys. Res.*, 113, D16S45, doi:10.1029/2007JD008988, 2008.

van der Werf, G. R., Morton, D. C., DeFries, R. S., Giglio, L., Randerson, J. T., Collatz, G. J., and Kasibhatla, P. S.: Estimates of fire emissions from an active deforestation region in the southern Amazon based on satellite data and biogeochemical modelling, *Biogeosciences*, 6, 235–249, doi:10.5194/bg-6-235-2009, 2009.

van Donkelaar, A., Martin, R. V., Pasch, A. N., Szykman, J. J., Zhang, L., Wang, Y. X., and Chen, D.: Improving the accuracy of daily satellite-derived ground-level fine aerosol concentration estimates for North America, *Environ. Sci. Technol.*, 46, 11971–11978, 2012.

Winer, A. M., Peters, J. W., Smith, J. P., and Pitts Jr., J. N.: Response of commercial chemiluminescent NO-NO<sub>2</sub> analyzers to other nitrogen containing compounds, *Environ. Sci. Technol.*, 8, 1118–1121, 1974.

Zhou, Y., Brunner, D., Boersma, K. F., Dirksen, R., and Wang, P.: An improved tropospheric NO<sub>2</sub> retrieval for OMI observations in the vicinity of mountainous terrain, *Atmos. Meas. Tech.*, 2, 401–416, doi:10.5194/amt-2-401-2009, 2009.

Zhou, Y., Brunner, D., Spurr, R. J. D., Boersma, K. F., Sneep, M., Popp, C., and Buchmann, B.: Accounting for surface reflectance anisotropy in satellite retrievals of tropospheric NO<sub>2</sub>, *Atmos. Meas. Tech.*, 3, 1185–1203, doi:10.5194/amt-3-1185-2010, 2010.

## Improved satellite retrievals of NO<sub>2</sub> and SO<sub>2</sub> over the Canadian oil sands

C. A. McLinden et al.

Title Page

Abstract

Introduction

Conclusions

References

Tables

Figures

◀

▶

◀

▶

Back

Close

Full Screen / Esc

Printer-friendly Version

Interactive Discussion

**Table 1.** Summary of air mass factor input parameters.

Parameter	Source	Horizontal resolution	Intra-annual variability	Interannual variability
Absorber profiles (NO <sub>2</sub> , SO <sub>2</sub> )	GEM-MACH + GEOS-CHEM	15 km × 15 km	Monthly	No <sup>a</sup>
Temperature profiles	GEM-MACH	15 km × 15 km	Monthly	No
Surface reflectivity (snow-free)	MODIS + OMI	0.05° × 0.05°; smoothed to 15 km × 30 km	Monthly	Yes
Surface reflectivity (snow)	MODIS	0.05° × 0.05°; smoothed to 15 km × 30 km	None	No
Ozone column	OMI (TOMS algorithm)	Single-value	Daily	Yes
Surface pressure	GEM-MACH	15 km × 15 km	Monthly	No

<sup>a</sup> As a sensitivity study, NO<sub>2</sub> profiles in the planetary boundary layer were doubled to account to approximate the effect of increasing emissions (see Sect. 4.1).

## Improved satellite retrievals of NO<sub>2</sub> and SO<sub>2</sub> over the Canadian oil sands

C. A. McLinden et al.

[Title Page](#)

[Abstract](#)

[Introduction](#)

[Conclusions](#)

[References](#)

[Tables](#)

[Figures](#)

[⏪](#)

[⏩](#)

[◀](#)

[▶](#)

[Back](#)

[Close](#)

[Full Screen / Esc](#)

[Printer-friendly Version](#)

[Interactive Discussion](#)

**Table 2.** Air mass factor look-up table nodes.

Parameter	Number of nodes	Table type	Node values
Altitude	30	Both	0 to 16 km in 0.5 km in layers
Surface Albedo	10	Clear-sky	0, 0.03, 0.06, 0.09, 0.12, 0.20, 0.30, 0.50, 0.75, 1.00
Column ozone	5	Both	275, 325, 375, 425, 475 DU
Surface Pressure	4	Clear-sky	600, 800, 900, 1000 hPa
Cloud top pressure	5	Cloudy	200, 400, 600, 800, 900 hPa
Solar Zenith Angle	10	Both	0, 30°, 50°, 60°, 65°, 70°, 73°, 76°, 78°, 80°
Viewing Zenith Angles	7	Both	0, 30°, 50°, 60°, 65°, 70°, 72°
Change in azimuthal angle	7	Both	0 to 180° in 30° increments



## Improved satellite retrievals of NO<sub>2</sub> and SO<sub>2</sub> over the Canadian oil sands

C. A. McLinden et al.

Title Page

Abstract

Introduction

Conclusions

References

Tables

Figures

⏪

⏩

◀

▶

Back

Close

Full Screen / Esc

Printer-friendly Version

Interactive Discussion



**Table 4.** Summary of comparisons between WBEA and OMI-EC-derived long-term (2005–2011) average volume mixing ratios. The slope and correlation coefficient are based on a sample of 12 SO<sub>2</sub> stations and 8 NO<sub>2</sub> stations.

Species	Slope	Correlation coefficient
NO <sub>2</sub>	0.20	0.45
– Millenium station	0.54	0.80
+ smoothing correction	0.56	0.90
+ clear-sky bias correction	0.65	0.91
Apr–Sep <sup>1</sup>	1.00	0.94
Oct–Mar <sup>1</sup>	0.47	0.68
SO <sub>2</sub>	0.88	0.91
+ smoothing correction	1.15	0.91
+ clear-sky bias correction	1.01	0.91

<sup>1</sup> Includes corrections for smoothing and clear-sky bias; excludes Millenium station.



**Fig. 1. (a)** Map of the Canada showing the oil sands area (tan) and the location of the surface mining (red) which also corresponds to the area shown in panels **(b)** and **(c)**. Panels **(b)** and **(c)** show Landsat images from 2005 and 2011 of the surface mining area (<http://earthobservatory.nasa.gov/Features/WorldOfChange/athabasca.php?all=y>). The white outlines denote the approximate boundaries of the main mining operations (as of 2011). The communities of Fort McMurray and Fort McKay are also indicated. The red dot denotes the reference location (57.1° N, 111.6° W). These panels cover approximately 90 km in both NS and EW directions.

## Improved satellite retrievals of NO<sub>2</sub> and SO<sub>2</sub> over the Canadian oil sands

C. A. McLinden et al.

Title Page

Abstract

Introduction

Conclusions

References

Tables

Figures

◀

▶

◀

▶

Back

Close

Full Screen / Esc

Printer-friendly Version

Interactive Discussion

## Improved satellite retrievals of NO<sub>2</sub> and SO<sub>2</sub> over the Canadian oil sands

C. A. McLinden et al.

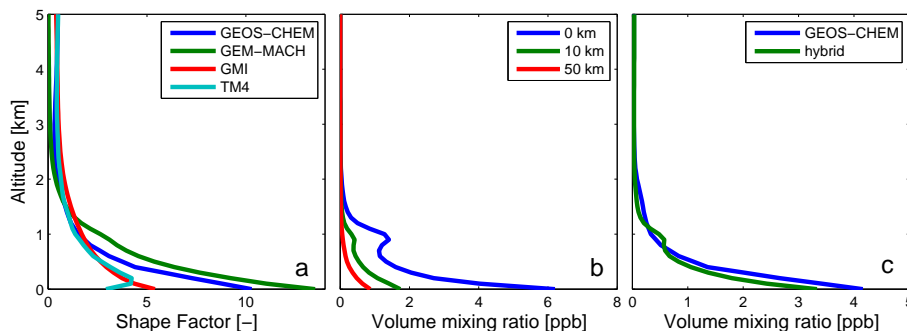


**Fig. 2.** Comparison of annual-mean model NO<sub>2</sub> profiles over the oil sands (sampled at the local time of the OMI overpass, ~ 13:30 LT): **(a)** TM4, GMI, GEOS-CHEM, and GEM-MACH shape factors each at a resolution of roughly 200 km (N–S) × 150 km (E–W), **(b)** GEM-MACH number density profiles (at its native 15 km × 15 km resolution) at distances of 0, 10, and 50 km from the reference location, and **(c)** GEOS-CHEM and the GEOS-CHEM+GEM-MACH hybrid (see text) profiles over the surface mines at a resolution of 0.5° × 0.67°.

Title Page

Abstract

Introduction

Conclusions

References

Tables

Figures

◀

▶

◀

▶

Back

Close

Full Screen / Esc

Printer-friendly Version

Interactive Discussion

## Improved satellite retrievals of NO<sub>2</sub> and SO<sub>2</sub> over the Canadian oil sands

C. A. McLinden et al.

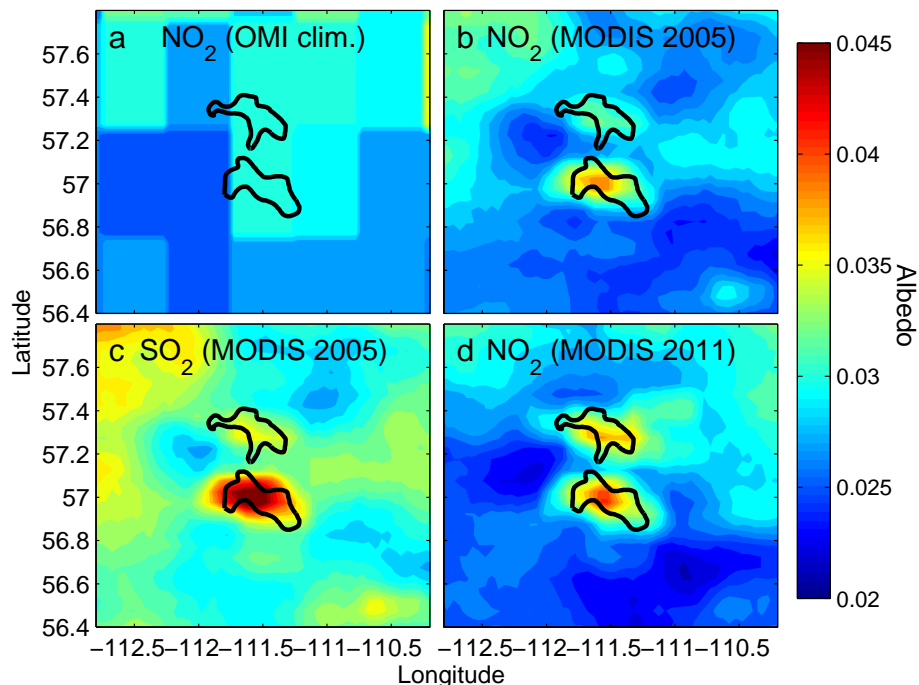


**Fig. 3.** Comparison of mean summer (JJA) surface albedos: **(a)** OMI climatological albedo at 442 nm (Kleipool et al., 2007), **(b)** MODIS albedo for 2005 from Eq. (3) for NO<sub>2</sub> (477 nm but scaled to 442 nm), **(c)** MODIS albedo for 2005 from Eq. (3) for SO<sub>2</sub> (477 nm but scaled to 354 nm), and **(d)** MODIS albedo for 2011 from Eq. (3) for NO<sub>2</sub> (477 nm but scaled to 442 nm). Each map shows the approximate outline of the surface mining region.

Title Page

Abstract Introduction

Conclusions References

Tables Figures

◀ ▶

◀ ▶

Back Close

Full Screen / Esc

Printer-friendly Version

Interactive Discussion

## Improved satellite retrievals of NO<sub>2</sub> and SO<sub>2</sub> over the Canadian oil sands

C. A. McLinden et al.

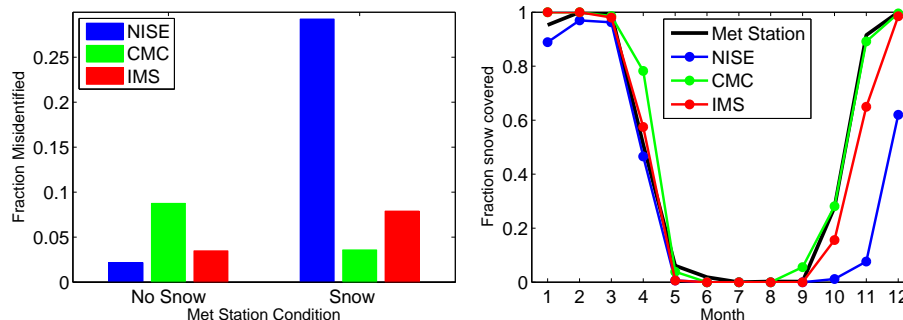


**Fig. 4.** Left: Fraction of days in which the snow cover product misidentified the presence of snow on the ground, relative to the determination from the meteorological station. Right: Monthly-mean fraction of days with snow as determined to be on the ground according to four source of data. These results are averaged over 2000–2011 and combined results from the Fort McMurray and Mildred Lake meteorological stations.

## Improved satellite retrievals of NO<sub>2</sub> and SO<sub>2</sub> over the Canadian oil sands

C. A. McLinden et al.

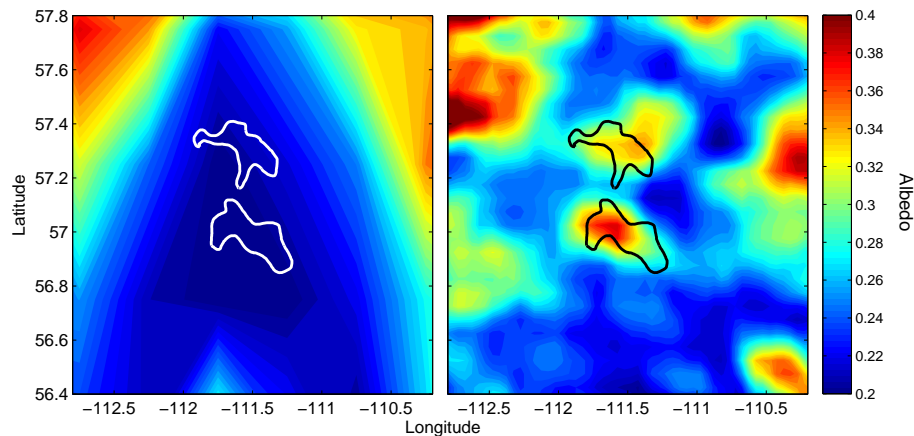


**Fig. 5.** Snow albedo over the oil sands surface mining region from: **(a)** OMI at at 354 nm and on a  $0.5^\circ \times 0.5^\circ$  grid (O’Byrne et al., 2010) and **(b)** MODIS at 477 nm smoothed to  $30 \text{ km} \times 15 \text{ km}$ .

[Title Page](#)[Abstract](#)[Introduction](#)[Conclusions](#)[References](#)[Tables](#)[Figures](#)[◀](#)[▶](#)[◀](#)[▶](#)[Back](#)[Close](#)[Full Screen / Esc](#)[Printer-friendly Version](#)[Interactive Discussion](#)

Improved satellite retrievals of  $\text{NO}_2$  and  $\text{SO}_2$  over the Canadian oil sands

C. A. McLinden et al.

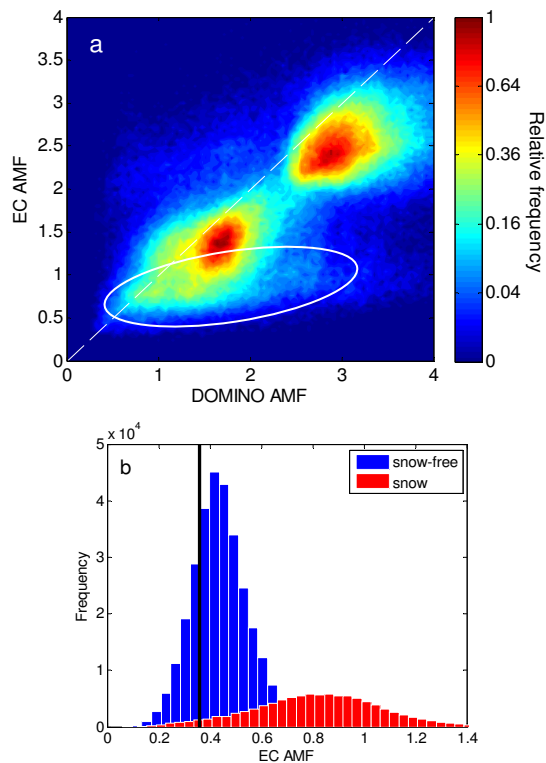


**Fig. 6. (a)** Scatterplot of DOMINOv2 vs. EC  $\text{NO}_2$  AMFs for all OMI observations within 200 km of the reference location and radiative cloud fraction of 0.2 or smaller. Note the non-linear scale. The white ellipse shows the AMFs over the surface mines (a small overall fraction of the points considered here). **(b)** Histogram of  $\text{SO}_2$  AMFs within 200 km of the reference location, separated according to snow covered surface, and snow-free. The black line indicates the constant AMF of 0.36 used in the NASA  $\text{SO}_2$  product.

## Improved satellite retrievals of NO<sub>2</sub> and SO<sub>2</sub> over the Canadian oil sands

C. A. McLinden et al.

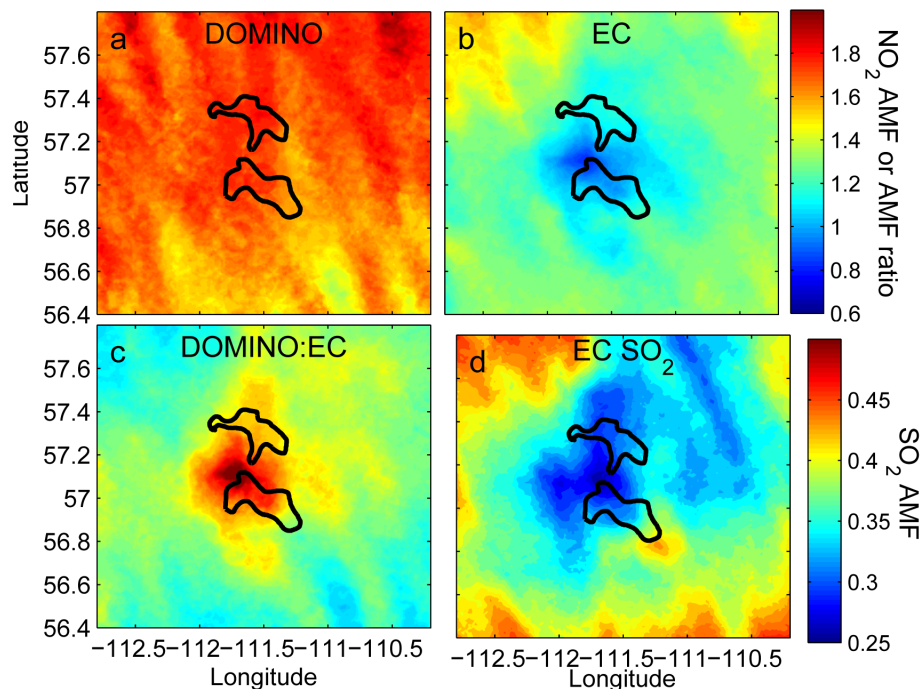


**Fig. 7.** Summertime air mass factors (AMFs) averaged over 2005–2011: **(a)** from the DOMINOv2 data files, **(b)** EC-AMF, **(c)** the ratio of DOMINOv2:EC which also represents the scaling that would be applied to the VCDs (the maximum is 1.4), and **(d)** EC SO<sub>2</sub> AMFs. These data have been averaged in the. The stripes arise due to sampling differences by the OMI sampling.

[Title Page](#)
[Abstract](#)
[Introduction](#)
[Conclusions](#)
[References](#)
[Tables](#)
[Figures](#)
[Back](#)
[Close](#)
[Full Screen / Esc](#)
[Printer-friendly Version](#)
[Interactive Discussion](#)

## Improved satellite retrievals of NO<sub>2</sub> and SO<sub>2</sub> over the Canadian oil sands

C. A. McLinden et al.

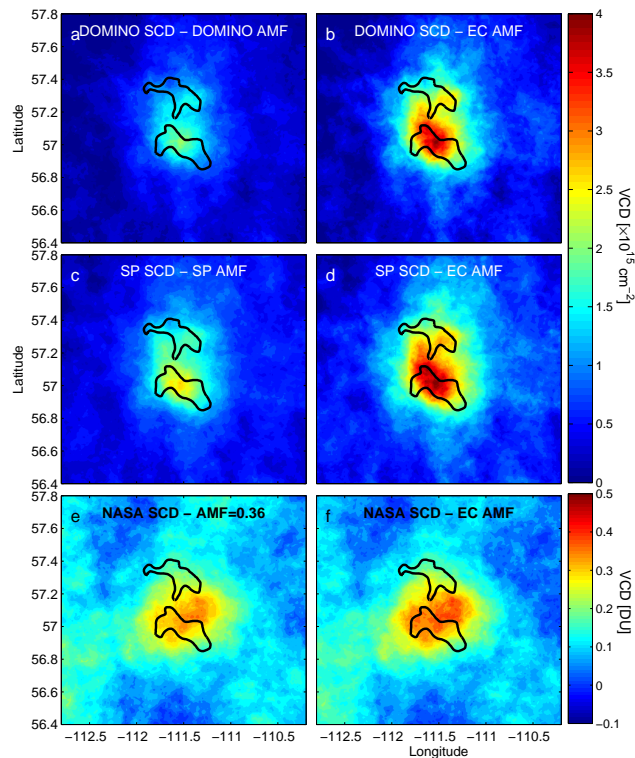


**Fig. 8.** Average (2005–2011) tropospheric VCDs: **(a)** DOMINO v2 NO<sub>2</sub>, **(b)** EC NO<sub>2</sub> (from DOMINO) **(c)** SP v2 NO<sub>2</sub>, **(d)** EC NO<sub>2</sub> (from SP), **(e)** NASA SO<sub>2</sub>, **(f)** EC SO<sub>2</sub>.

## Improved satellite retrievals of NO<sub>2</sub> and SO<sub>2</sub> over the Canadian oil sands

C. A. McLinden et al.

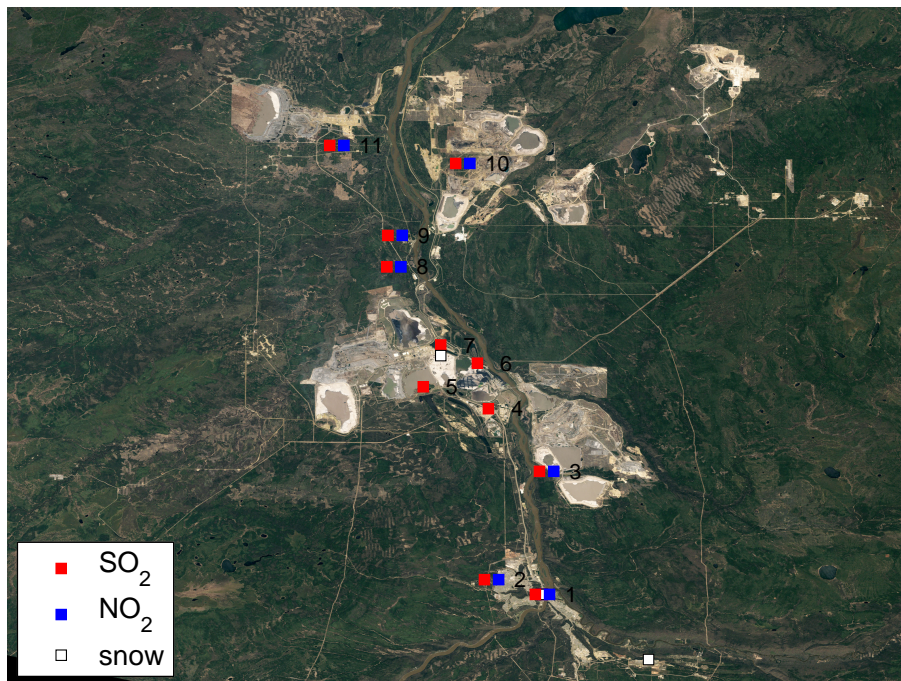


**Fig. 9.** Map of Wood Buffalo Environment Association (WBEA) monitoring stations and the parameters measured (<http://earthobservatory.nasa.gov/Features/WorldOfChange/athabasca.php?all=y>). A 12th site (Fort Chippewyan), measuring SO<sub>2</sub> and NO<sub>2</sub>, is located approximately 160 km north of site 10. Additional information on these sites can be found in the Supplement.

Title Page

Abstract

Introduction

Conclusions

References

Tables

Figures

◀

▶

◀

▶

Back

Close

Full Screen / Esc

Printer-friendly Version

Interactive Discussion

## Improved satellite retrievals of NO<sub>2</sub> and SO<sub>2</sub> over the Canadian oil sands

C. A. McLinden et al.

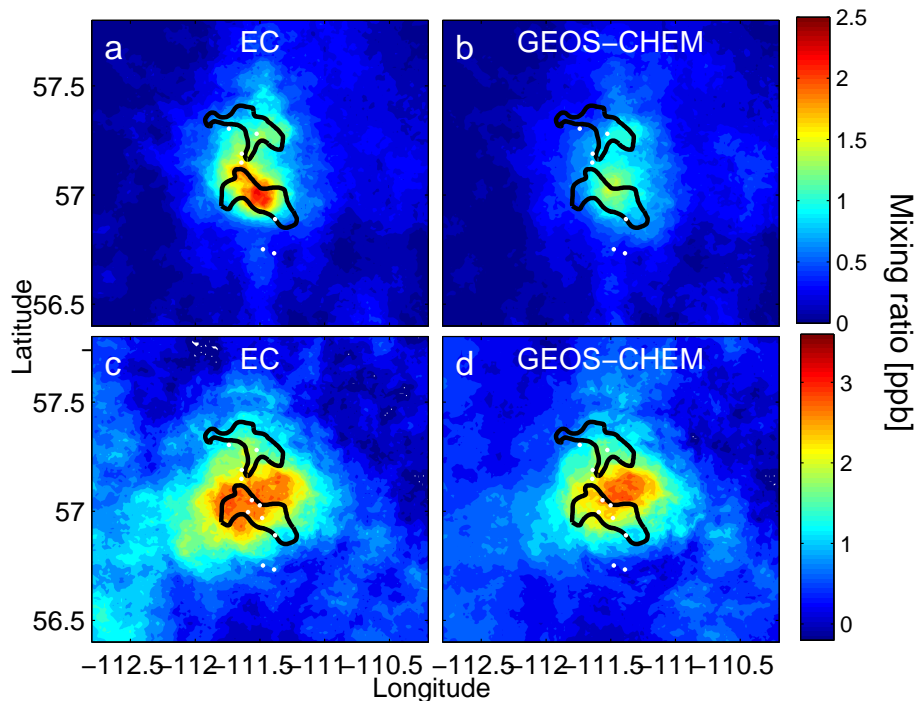


**Fig. 10.** Average (2005–2011) EC-OMI distributions of NO<sub>2</sub> and SO<sub>2</sub> vmr: **(a)** EC-OMI NO<sub>2</sub>, **(b)** as **(a)** but using GEOS-CHEM profiles to calculate AMFs and the column to surface mapping, **(c)** EC-OMI SO<sub>2</sub>, **(d)** as **(c)** but using GEOS-CHEM profiles to calculate AMFs and the column to surface mapping. The points indicate the location of the NO<sub>2</sub> and SO<sub>2</sub> in-situ instruments.

Improved satellite retrievals of NO<sub>2</sub> and SO<sub>2</sub> over the Canadian oil sands

C. A. McLinden et al.

Title Page

Abstract

Introduction

Conclusions

References

Tables

Figures

◀

▶

◀

▶

Back

Close

Full Screen / Esc

Printer-friendly Version

Interactive Discussion

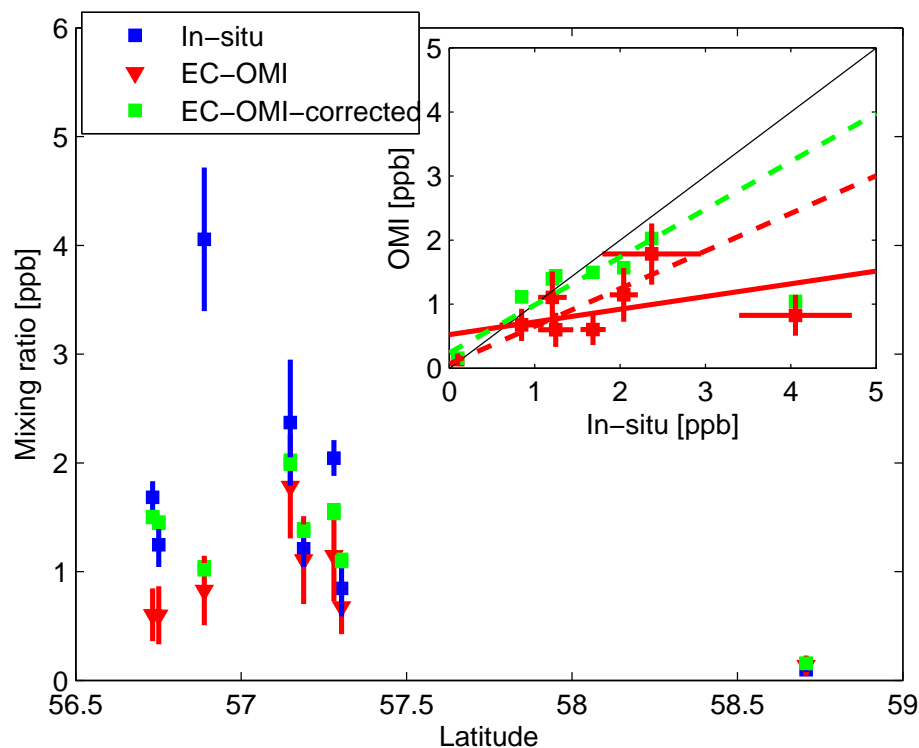


**Fig. 11.** Average (2005–2011) ground-based in-situ and EC-OMI-derived NO<sub>2</sub> surface mixing ratio measurements as a function of WBEA station latitude. Inset is the scatter-plot comparing ground-based with EC-vmrs. The red represents original OMI-vmrs while the green is after accounting for smoothing and clear-sky bias. Errors bars denote twice the standard error of the mean. The ground-based measurements have been corrected for the interference effect and include this uncertainty in their error bars (see Table S1). The lines in the inset represent the linear fits with (solid) and without (dashed) including the Millennium station (#3).

## Improved satellite retrievals of NO<sub>2</sub> and SO<sub>2</sub> over the Canadian oil sands

C. A. McLinden et al.

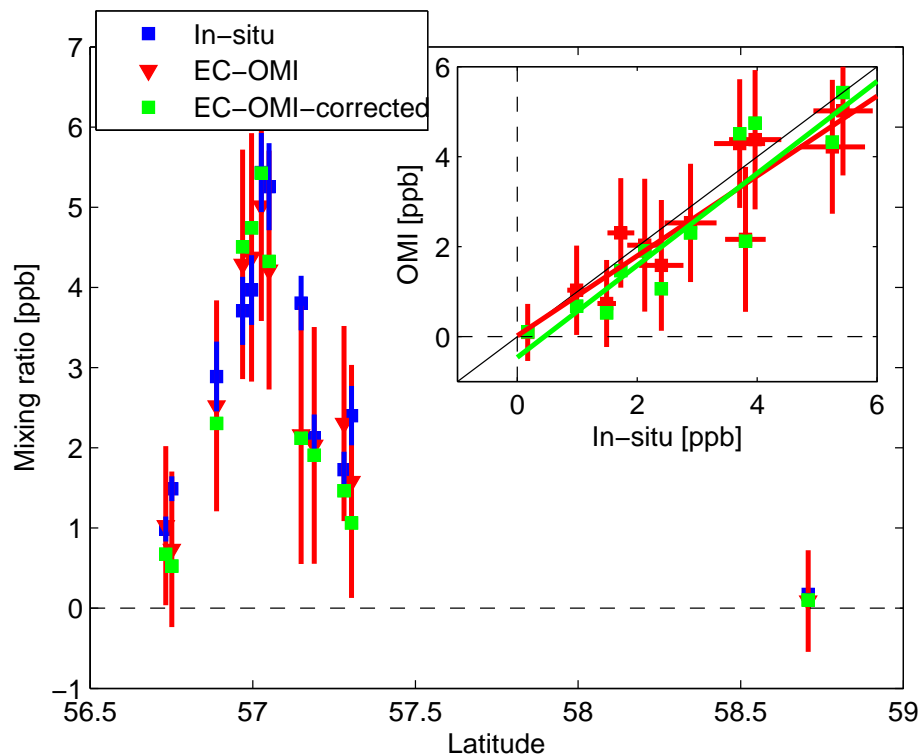


**Fig. 12.** Average (2005–2011) ground-based in-situ and EC-VMR-derived SO<sub>2</sub> surface mixing ratio measurements as a function of WBEA station latitude. Inset is the scatter-plot comparing ground-based with EC-vmrs. The red represents original OMI-vmrs while the green is after accounting for smoothing and clear-sky bias. Errors bars denote twice the standard error of the mean.

[Title Page](#)[Abstract](#)[Introduction](#)[Conclusions](#)[References](#)[Tables](#)[Figures](#)[◀](#)[▶](#)[◀](#)[▶](#)[Back](#)[Close](#)[Full Screen / Esc](#)[Printer-friendly Version](#)[Interactive Discussion](#)